Fermilab Proposal E-871/97

Proposal to Continue the Study of Hyperon CP Violation in FY99

The HyperCP Collaboration

December 14, 1997

A. Chan, Y.C. Chen, J. Sheng, P.K. Teng, C. Yu, and Z. Yu
Academia Sinica, Nankang, Taipei 11529, Taiwan, Republic of China

W.S. Choong, G. Gidal, K.B. Luk[1], and P. Zyla
Lawrence Berkeley Laboratory and University of California, Berkeley, CA 94720, USA

M. Crisler, C. James and J. Volk
Fermilab, Batavia, IL 60510, USA

J. Felix, G. Lopez
Universidad de Guanajuato, León, Mexico

R.A. Burnstein, A. Chakravorty, D.M. Kaplan, L.M. Lederman, W. Luebke, D. Rajaram, H.A. Rubin, C.G. White, and S.L. White
Illinois Institute of Technology, Chicago, IL 60616, USA

N. Leros and J.-P. Perroud
Université de Lausanne, Lausanne, Switzerland

H.R. Gustafson, M.J. Longo, and F. Lopez
University of Michigan, Ann Arbor, MI 48109, USA

V. Papavassiliou
New Mexico State University, Las Cruces, NM 88003, USA

M. Jenkins and K. Clark
University of South Alabama, Mobile, AL 36688, USA

M. Carmack, E.C. Dukes[2], C. Durandet, T. Holmstrom, M. Huang, Z. Kou, and K.S. Nelson
University of Virginia, Charlottesville, VA 22901, USA

[1]Spokesperson: LUK@CSA.LBL.GOV, (510)486-7054
[2]Spokesperson: DUKES@UVAHEP.PHYS.VIRGINIA.EDU, (804)982-5364

We pray for the second coming of CP *violation ...*

A. Pais

Summary

In September 1997 the HyperCP (E871) collaboration completed a first run of a study of CP violation in Λ ($\overline{\Lambda}$) and Ξ^- ($\overline{\Xi}^+$) decays. Despite a very aggressive schedule and limited data-taking time, the run was a great success. In two years we built from scratch a hyperon beam and the highest rate spectrometer in the world and used it to accumulate by far the largest sample of hyperon decays. We expect to attain a statistical precision of 2×10^{-4} in the sum of the Λ and Ξ CP asymmetries, two orders of magnitude better than the present limit, and where some theories predict an effect. A non-zero asymmetry would be unambiguous evidence of direct CP violation and the first evidence of CP violation outside of the decay of K_L^0. The collaboration will also make sensitive studies of various rare and forbidden hyperon decays.

The upcoming Tevatron run with the Main Injector will allow us to take advantage of what has been learned from the first run to increase substantially our data sample and improve the quality of the data. Simple improvements to the data acquisition system, modest increases in secondary beam rates, and a new spill structure should permit at least a fourfold increase in statistics and allow us to reach an uncertainty of 1×10^{-4} or better in the hyperon CP asymmetry. Besides increasing our yields, we expect a substantial improvement in the quality of the data due to a number of modest, but significant, improvements in the apparatus and the monitoring software, and a better understanding of our spectrometer.

Contents

1 Introduction

The HyperCP collaboration has undertaken an ambitious effort to observe CP violation in Ξ and Λ hyperon decays at Fermilab. Construction of a new hyperon beam and a fast, new, state-of-the-art detector — to our knowledge, the highest rate spectrometer in the world — was completed in the fall of 1996, and a successful first run of the experiment ended in September 1997. We have accumulated about 75 billion events — the largest data sample ever taken in a HEP experiment — which will enable us to probe CP violation in hyperon decays two orders of magnitude beyond the current limit. *In only 2 hours of running the HyperCP spectrometer accumulated more Ξ^- and $\overline{\Xi}^+$ events than all previous experiments.*

Observation of CP violation in this experiment would be the first evidence of CP violation outside of the decay of the K_L^0 and unambiguous evidence of direct CP violation. We have also accumulated an enormous sample of charged kaon decays which will allow a sensitive search for CP violation in $K^\pm \rightarrow \pi^\pm\pi^\pm\pi^\mp$ decays. And finally, the experiment will perform a high-statistics search for rare and forbidden hyperon decays and charged kaon decays.

A second run of the experiment will allow us to build on the success of the first run, taking advantage of what we have learned about our spectrometer to increase both the quantity and quality of the data. We expect to increase our data sample by at least a factor of four to achieve a precision of 1×10^{-4} or better in the CP asymmetry. Most of the increase in yield will simply come from running at the intensity and efficiency that we attained at the end of the 1997 fixed-target run. The quality of the data will also be significantly improved by modest improvements to the apparatus and by better online monitoring software.

We should emphasize that future runs of the experiment at Main Injector energies would not be fruitful due to the much lower hyperon yields at 120 GeV and intractable systematic errors at lower energies.

In the following sections we first briefly review the physics of CP violation in hyperon decays. (Other physics topics the collaboration will study are described in Appendix A.) We then describe the spectrometer and how well it performed in the 1997 fixed-target run. The 1997 run is summarized and preliminary results are given. Finally we outline our expectations for the FY99 run and how we propose to achieve them.

2 Physics of Hyperon CP Violation

The central idea of our hyperon CP violation experiment is simple. We compare the Λ and $\overline{\Lambda}$ decay distributions in the following reactions:

$$\begin{array}{lll} \Xi^- \to \Lambda^0\,\pi^- & \quad\text{and}\quad & \overline{\Xi}^+ \to \overline{\Lambda}^0\,\pi^+ \\ \quad\hookrightarrow p\,\pi^- & & \quad\hookrightarrow \overline{p}\,\pi^+, \end{array}$$

where the Ξ^- and $\overline{\Xi}^+$ hyperons are produced unpolarized. Any difference in these distributions is unambiguous evidence of direct CP violation.

2.1 Signatures for CP Violation in Hyperon Decays

Because the non-leptonic weak decays of spin-$\frac{1}{2}$ hyperons violate parity, they can decay into admixtures of both S- and P-wave final states. In terms of the S- and P-wave amplitudes, the hyperon nonleptonic decays are conventionally described by the Lee–Yang variables α, β, and γ [1]:

$$\alpha = \frac{2\mathrm{Re}(S^*P)}{|S|^2+|P|^2}, \qquad \beta = \frac{2\mathrm{Im}(S^*P)}{|S|^2+|P|^2}, \qquad \gamma = \frac{|S|^2-|P|^2}{|S|^2+|P|^2}, \tag{1}$$

where $\alpha^2+\beta^2+\gamma^2=1$. The decay distribution of the daughter spin-$\frac{1}{2}$ baryon in the rest frame of the parent hyperon (the proton in the decay $\Lambda \to \mathrm{p}\pi^-$, for example) is not isotropic, because of parity violation, but is given by:

$$\frac{dP}{d\Omega} = \frac{1}{4\pi}(1+\alpha\vec{P}_p\cdot\hat{p}_d), \tag{2}$$

where $\vec{P}_p$ is the parent hyperon polarization and $\hat{p}_d$ is the daughter baryon momentum direction in the rest frame of the parent. As shown in Fig. 1, protons are predominantly emitted in the direction of the Λ polarization and antiprotons are predominantly emitted in the direction opposite to the $\overline{\Lambda}$ polarization.

If CP is conserved then, as shown in Fig. 1, $\alpha = -\overline{\alpha}$, where the overlined quantity refers to the antihyperon. Hence the observable sensitive to CP violation is[1]:

$$A = \frac{\alpha+\overline{\alpha}}{\alpha-\overline{\alpha}}. \tag{3}$$

Measuring the alpha parameter in a hyperon decay is done by measuring the slope of the daughter $\cos\theta$ distribution in the frame where the parent polarization defines the polar axis. That distribution is given by:

$$\frac{dN}{d\cos\theta} = \frac{1}{2}(1+P_p\alpha_p\cos\theta), \tag{4}$$

[1]There are other observables sensitive to CP violation but none of them is as experimentally accessible as α. See the P-871 proposal for details about these other CP observables.

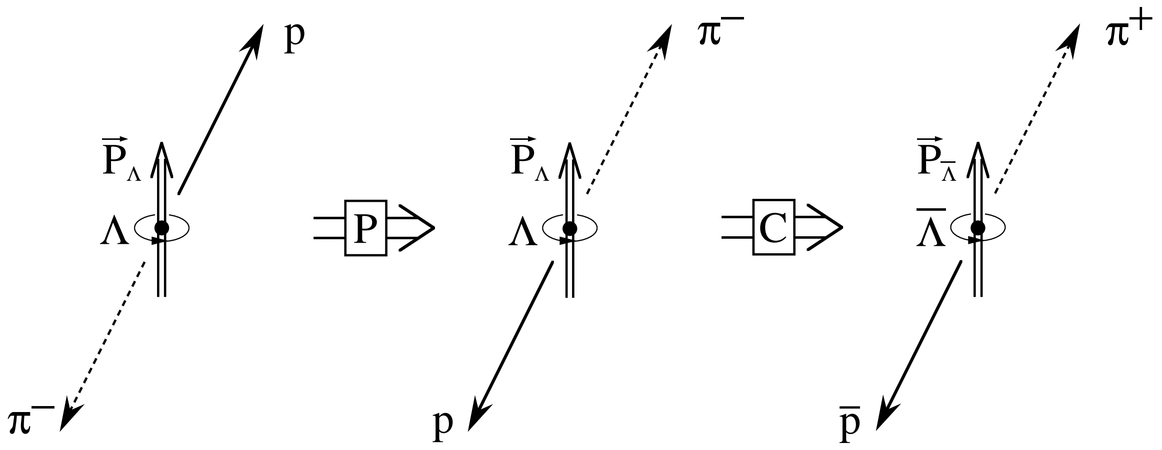

Figure 1: Λ decay under P and C transformations.

where θ is the angle between the parent polarization and the daughter momentum. *Since the slope of the* $\cos\theta$ *distribution is given by the product* $P_p\alpha_p$*, the alpha parameter can only be extracted if the parent polarization is known.*

How HyperCP produces hyperons of a well-known polarization is as follows. In HyperCP we measure the proton and antiproton $\cos\theta$ distributions from Λ and $\overline{\Lambda}$ hyperons that are produced from Ξ^- and $\overline{\Xi}^+$ decays. In general the polarization of the daughter baryon in a non-leptonic spin-$\frac{1}{2}$ hyperon decay is given by:

$$\vec{P}_d = \frac{(\alpha + \vec{P}_p \cdot \hat{p}_d)\hat{p}_d + \beta(\vec{P}_p \times \hat{p}_d) + \gamma[\hat{p}_d \times (\vec{P}_p \times \hat{p}_d)]}{1 + \alpha\vec{P}_p \cdot \hat{p}_d}. \tag{5}$$

If the parent hyperon is unpolarized then this equation simplifies to:

$$\vec{P}_d = \alpha\,\hat{p}_d. \tag{6}$$

We produce Ξ^- and $\overline{\Xi}^+$ hyperons through the reaction p + Cu $\rightarrow \Xi^\pm + X$. Because of parity conservation in strong interactions and because the hyperons are produced with $p_t \cong 0$, the Ξ's must be unpolarized. As a consequence, the daughter Λ is in a helicity state with polarization given by the alpha parameter of Ξ:

$$\vec{P}_\Lambda = \alpha_\Xi \hat{p}_\Lambda. \tag{7}$$

We can now re-write Eq. 4 in the frame in which the Λ polarization defines the polar axis as (Λ helicity frame — see Fig. 2)

$$\frac{dN}{d\cos\theta} = \frac{1}{2}(1 + \alpha_\Xi\alpha_\Lambda\cos\theta), \tag{8}$$

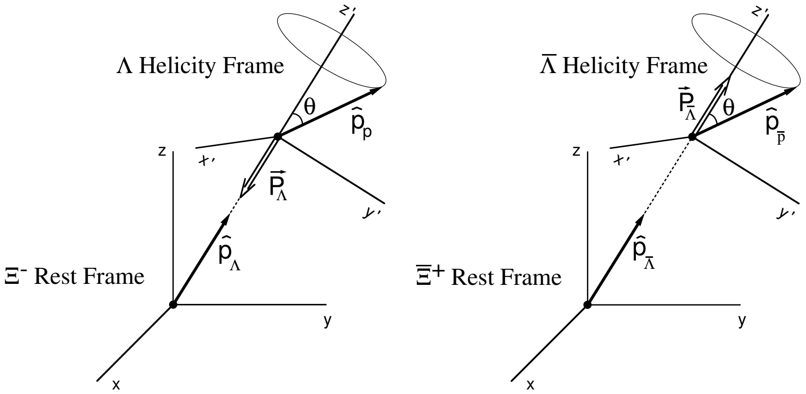

Figure 2: Analysis frames used in the Λ and $\overline{\Lambda}$ polarization analyses. The polar axis in the Λ rest frame (primed frame) is defined by the direction of the Λ momentum in the Ξ rest frame. The Λ and $\overline{\Lambda}$ have helicities of equal magnitude but opposite sign if CP is a good symmetry. However, since the sign of the Λ helicity reverses under CP, the probabilities of the proton and antiproton being emitted with polar angle θ are identical if CP is a good symmetry.

where θ is the angle between the proton momentum and the Λ polarization vector in the Λ rest frame. Hence, what we measure and compare are the products $\alpha_\Xi \alpha_\Lambda$ and $\alpha_{\overline{\Xi}} \alpha_{\overline{\Lambda}}$ which, *if CP is a good symmetry*, should be identical since both α_Ξ and α_Λ flip sign under CP.

We define the asymmetry parameter $A_{\Xi\Lambda}$, which is given by:

$$A_{\Xi\Lambda} = \frac{\alpha_\Xi \alpha_\Lambda - \alpha_{\overline{\Xi}} \alpha_{\overline{\Lambda}}}{\alpha_\Xi \alpha_\Lambda + \alpha_{\overline{\Xi}} \alpha_{\overline{\Lambda}}} \simeq A_\Xi + A_\Lambda, \tag{9}$$

and should be zero if CP is a good symmetry. HyperCP cannot distinguish whether an observed asymmetry originates in Ξ or Λ decay since α_Ξ and α_Λ are not measured separately. However, almost all theories (including the Standard Model) predict like signs for A_Ξ and A_Λ so the probability of any cancellation is remote [2].

2.2 Predictions

Model-independent expressions for the observable A have been explicitly calculated for various hyperon decays [3]. To leading order they are, for $\Lambda \to p\pi^-$ decay:

$$A_\Lambda \cong -\tan(\delta_1^P - \delta_1^S)\sin(\phi_1^P - \phi_1^S), \tag{10}$$

and for $\Xi^- \to \Lambda\pi^-$ decay:

$$A_\Xi \cong -\tan(\delta_3^P - \delta_3^S)\sin(\phi_1^P - \phi_1^S), \tag{11}$$

where ϕ are CP-violating weak phases, and δ are strong phase shifts.

Note that a difference in the S- and P-wave final-state interaction phases is essential in order for A to be non-zero. The $p\pi^-$ phase shifts have been measured, and $\delta_1^P - \delta_1^S = 7°$ with an error of about 1° [4]. The $\Lambda\pi$ phase shifts have not been measured and there is about an order of magnitude variation in the S-wave theoretical predictions (see [5] and [6]).

The magnitudes of the CP asymmetries in hyperon decays depend on the values of ϵ, ϵ', the top quark mass and the hadronic matrix elements. (Note that although limits on the magnitude of ϵ' constrain ϕ_1^S, they do not put any limits on ϕ_1^P, and hence on the asymmetry A [7].) Calculations are notoriously difficult, and *results are not reliable to better than an order of magnitude*, with the largest uncertainty due to the inability in determining the hadronic matrix elements.

The magnitudes of the predicted CP asymmetries are model dependent. In the Standard Model CP-violation effects are due solely to the complex phase in the CKM matrix, and hence hyperon CP asymmetries can only arise from matrix elements which involve transitions to the third quark generation. These are thought to be dominated by the gluon-penguin diagram for both kaon and hyperon decays [8]. (See Fig. 3). Theories with no $|\Delta S| = 1$, CP-odd effects, such as Superweak models and models with a very heavy neutral Higgs, predict no CP asymmetries. Models in which $|\Delta S| = 1$ CP nonconservation is dominant, such as the Weinberg model, predict asymmetries which are on the order of those calculated in the Standard Model. In Table 1 are shown some recent predictions for the CP asymmetries A_Ξ and A_Λ.

Table 1: Predictions of A_Ξ and A_Λ.

Model	A_Ξ $[10^{-4}]$	A_Λ $[10^{-4}]$	
CKM Model	$-(0.1-1)$	$-(0.1-0.5)$	[9]
Weinberg	≈ -3.2	≈ -0.25	[3]
Multi-Higgs (FCNE)	≈ 0	≈ 0	[9]
LR (isoconjugate)	≈ 0.5	≈ -0.11	[3]
LR (with mixing)	< 1	< 7	[7]

HyperCP has generated renewed theoretical interest in CP violation in hyperon decays. Recent papers by Pakvasa *et al.* [7], Wise *et al.* [5], Deshpande *et al.* [10], Valencia *et al.* [11], and Datta *et al.* [6], explicitly refer to HyperCP and anticipate our results. Our analysis technique has also been suggested as a means of looking for CP violation in beauty baryon decays in a paper by Albrecht *et al.* [12].

2.3 Comparison with Direct CP violation in Kaon Decays

A brief word about the difference between CP violation in kaons and hyperons. Although there is a close relationship between direct CP violation in kaon and hyperon decays, the differences are important. The most promising method of looking for direct CP violation in neutral kaons is by measuring ϵ'/ϵ. A non-zero value of ϵ'/ϵ is expressed through the interference of isospin $I = 0$ and $I = 2$ final states, whereas a non-zero value of A in hyperon decays is due to the interference between S-wave and P-wave final states. In Standard Model calculations the value of ϵ'/ϵ is very sensitive to the top quark mass whereas the hyperon CP asymmetry parameter A is not [13]. The reason for this sensitivity is the cancellation of the QCD and electroweak penguin diagrams [14]. Hence ϵ'/ϵ diminishes with increasing top mass and becomes negative at a top mass above around 200 GeV/c^2.

As mentioned above, measurements of ϵ' only set limits on the weak phase ϕ_1^S and not on ϕ_1^P — that is, a small value of ϵ' does not preclude a large value of A. Hence, to quote He and Valencia [11]:

> ...this measurement is complementary to the measurement of ϵ'/ϵ, in that it probes potential sources of CP violation at a level that has not been probed by the kaon experiments.

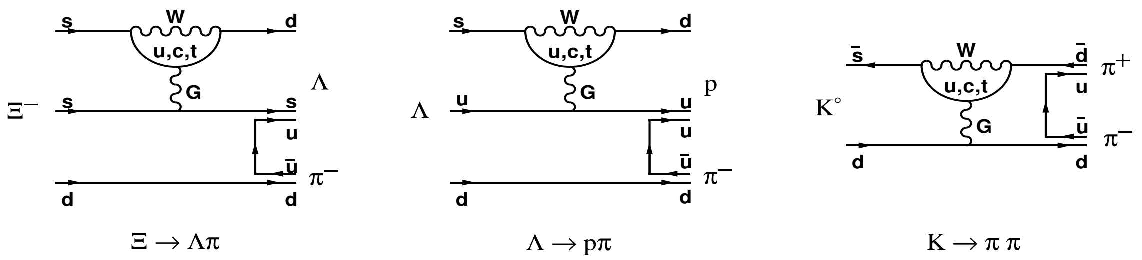

Figure 3: Gluon penguin diagrams responsible for $|\Delta S| = 1$ direct CP violation in $\Xi^- \to \Lambda\pi^-$, $\Lambda \to p\pi^-$, and $K \to \pi^+\pi^-$ decays. The electroweak penguin diagrams are identical except that the gluon is replaced by the γ and Z°.

2.4 Present Experimental Limits

The only data on CP violation in hyperon decays comes from the comparison of the alpha parameters in Λ and $\overline{\Lambda}$ decays. The experimental limits are weak. The three published results are given in Table 2. Each of the three experiments used a different technique, all were limited by statistical, not systematic errors, and none was a dedicated CP-violation experiment.

Table 2: Experimental results on $A_\Lambda = (\alpha_\Lambda + \alpha_{\overline{\Lambda}})/(\alpha_\Lambda - \alpha_{\overline{\Lambda}})$.

Mode	Result	Experiment
$\mathrm{pp} \rightarrow \Lambda\mathrm{X},\ \mathrm{\overline{p}p} \rightarrow \overline{\Lambda}\mathrm{X}$	0.02 ± 0.14	R608 [16]
$\mathrm{e^+e^-} \rightarrow \mathrm{J}/\psi \rightarrow \Lambda\overline{\Lambda}$	0.01 ± 0.10	DM2 [17]
$\mathrm{p\overline{p}} \rightarrow \Lambda\overline{\Lambda}$	0.010 ± 0.022	PS185 [18]

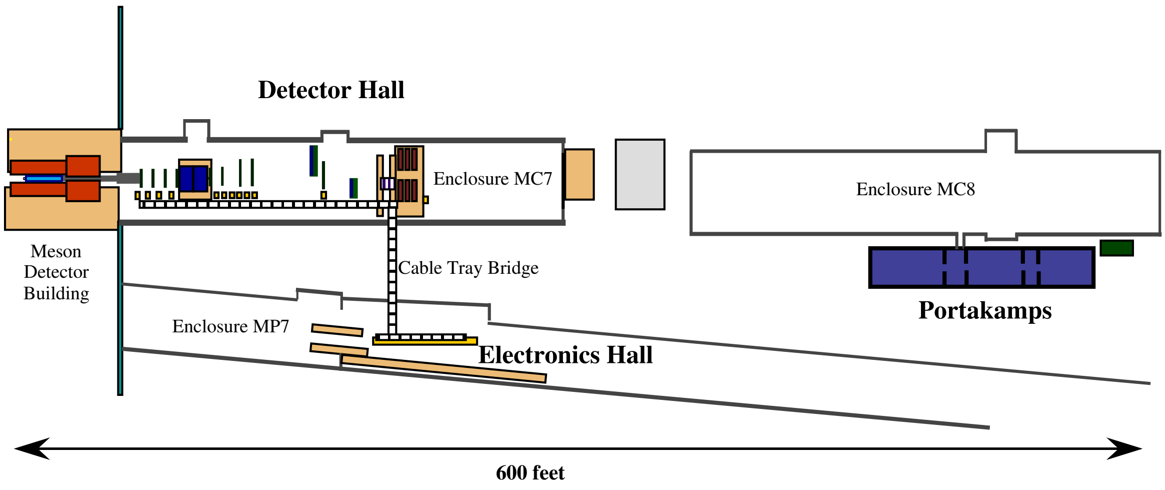

Figure 4: HyperCP experimental layout. The spectrometer rests in MC7, the front-end electronics are in MP7, and the data acquisition system and on-line computers are in the Portakamps.

3 Description and Performance of the Spectrometer in 1997

The layout of the experimental area is given in Fig. 4, and the plan and elevation views of the spectrometer are shown in Fig. 5. The spectrometer is in the Meson Center beam line at Fermilab. For reasons related to radiation safety and economics, the front-end and trigger electronics are in the neighboring beam line (MP), and the data acquisition system is in a Portakamp 100 m away.

CP violation in hyperon decays is best studied using a simple, high-rate spectrometer. High rate is required to achieve the necessary statistics, while simplicity is demanded to keep systematic effects small and controllable.

Ξ hyperons are produced by steering an 800 GeV proton beam into a 2 mm by 2 mm copper target, either 2 cm or 6 cm in length. Different target lengths are used to

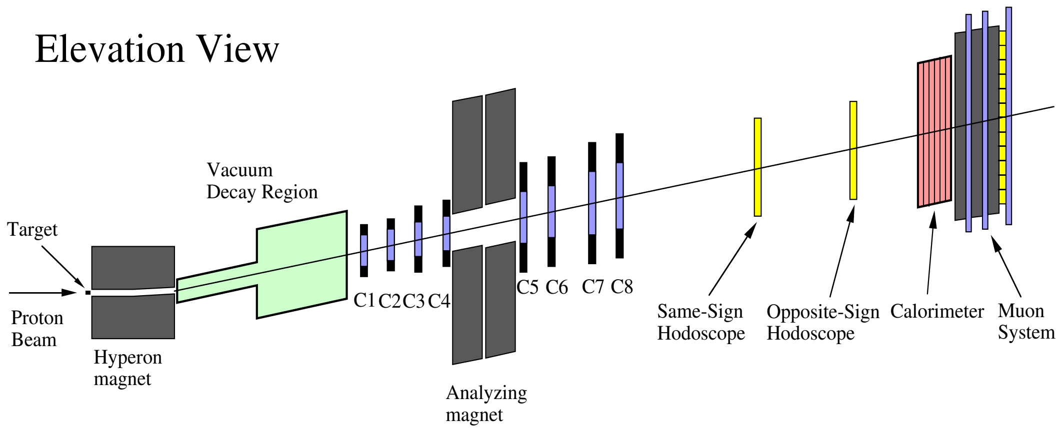

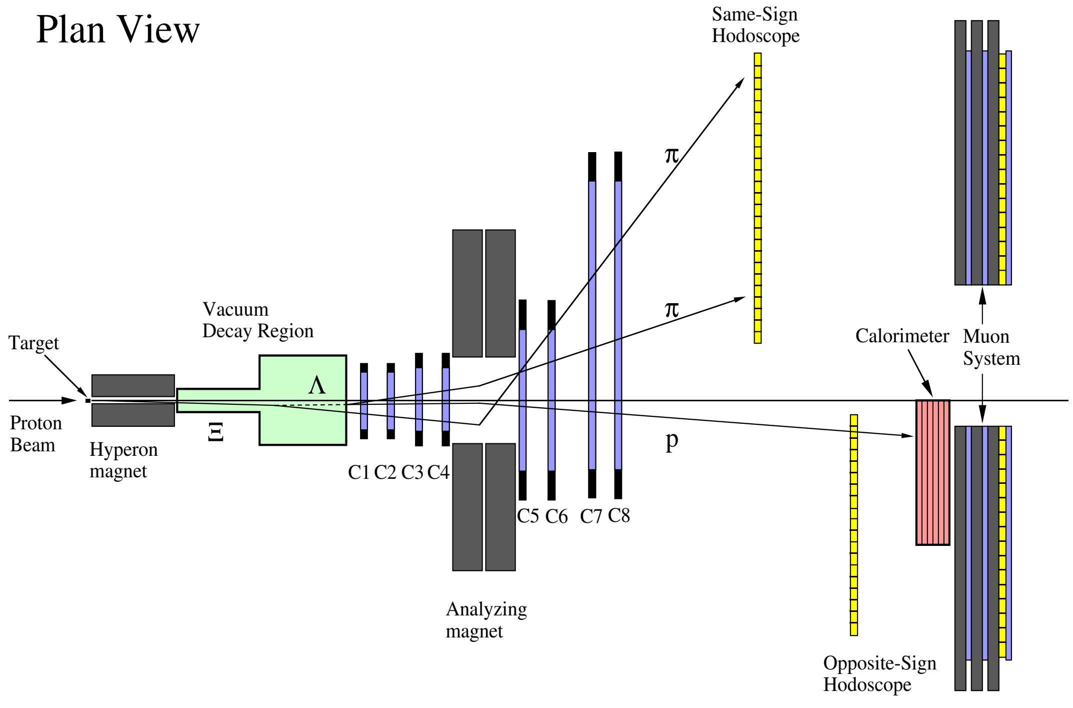

Figure 5: Plan and elevation views of the HyperCP apparatus.

equalize the secondary beam rate in the spectrometer between Ξ^- and $\overline{\Xi}^+$ runs. A 4.88 μsr collimator centered with the incoming proton beam and embedded within a 6 m long 1.67-T dipole magnet selects charged particles having an average momentum of about 170 GeV/c. To go from Ξ^- to $\overline{\Xi}^+$ running, the polarities of both the selection magnet and the spectrometer analysis magnet are reversed. A typical primary beam intensity of 1.5×10^{11} protons per spill gives a secondary beam rate of 20 MHz at the exit of the collimator. Upon exiting the collimator, the secondary beam traverses a 13 m long evacuated decay pipe after which it enters the spectrometer proper.

Immediately downstream of the decay region are four high-rate proportional wire chambers, followed by an analyzing magnet composed of two BM109 dipoles having a combined p_t kick of 1.43 GeV/c, followed by another four high-rate proportional wire chambers. The analysis magnet has sufficient strength to ensure that the protons and pions from the Ξ, Λ and K decays are always well separated from each other as well as from the charged beam in the downstream portion of the spectrometer. This allows a simple, yet selective, trigger to be formed by requiring the coincidence of charged particles in the hodoscopes at the rear of the spectrometer, on either side of the channeled beam. A hadronic calorimeter on the proton side is used to make the trigger "blind" to muons and to reduce the trigger rate from interactions of the channeled beam in the spectrometer. A simple muon system at the rear of the spectrometer allows access to rare and forbidden decays. To reduce multiple scattering and secondary interactions, helium bags are positioned between the detector components and within the analyzing magnet apertures.

The data are recorded with two data acquisition (DAQ) systems: a fast DAQ to read out events to tape and a slow DAQ used to read out the scalers and other beam-line information to disk. The fast DAQ reads data from two front-end latch systems: one for the spectrometer chambers and the other for the muon chambers. The data are transferred into a large (960 Mbyte) fast buffer via five parallel optical paths. The events are then built in parallel in five VME crates by 15 MVME167 single-board computers and written by 45 Exabyte 8505 tape drives. At the 20 MHz secondary-beam rate, the data acquisition system has a rate to tape of 13 Mbytes/s or approximately 75,000 events per second of beam.

3.1 Wire Chambers

The heart of the HyperCP spectrometer is eight high-rate, narrow-pitch multiwire proportional chambers (MWPC)[2]. All MWPCs have a similar construction; four anode wire planes are sandwiched by cathode foils and two outer grounded foils terminate the field region. The anode planes comprise two bend-view windings (X & X', shifted by half a wire spacing) and two windings inclined at $\pm 26.6°$ (U & V). All together the MWPC

[2]A ninth chamber, intended to provide an additional measurement of the high momentum daughter baryon position, had an insignificant effect on the mass resolution and was eventually used as a replacement chamber.

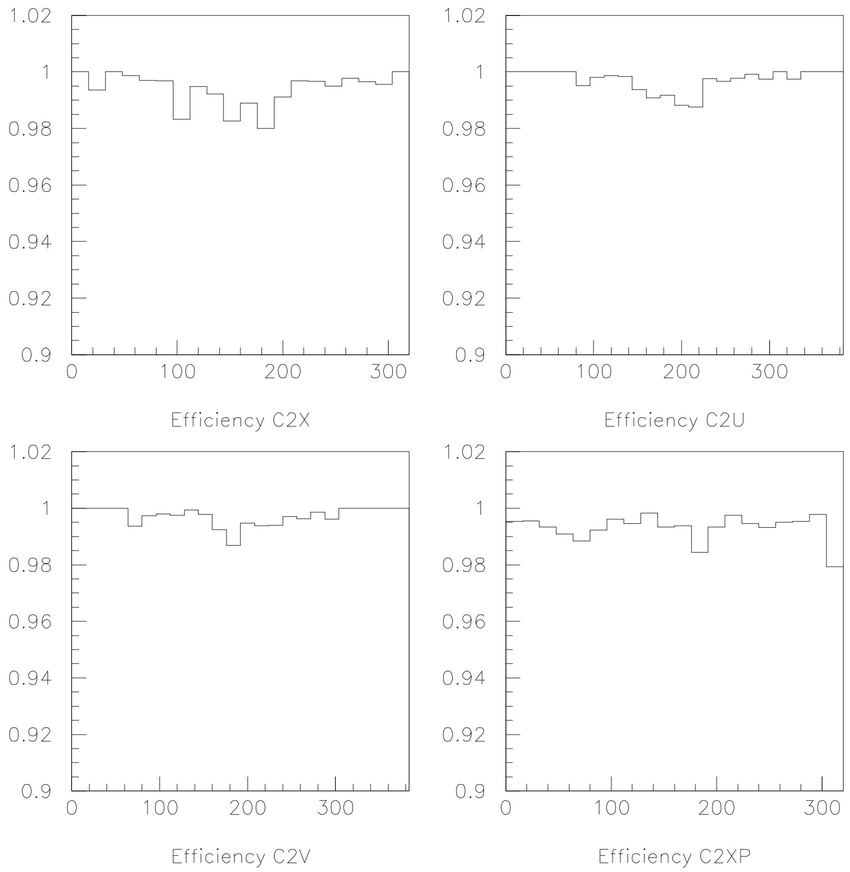

Figure 6: Localized chamber 2 efficiencies in groups of 16 wires at a channeled beam intensity of 20 MHz.

system comprises 18,752 instrumented wires.

The wire chambers all have small anode-cathode gaps (3 mm) and narrow wire spacings in order to perform efficiently and to have good aging properties in the intense secondary beam emanating from the collimator. For the majority of the 1997 run the total secondary beam rate through the chambers was about 20 MHz, corresponding to a typical individual wire rate of 0.4 MHz and a local flux of 0.5 MHz/cm^2 at the center of the most upstream chamber. The hyperon decay products inhabit the same region of the upstream wire chambers as the channeled beam while in the downstream chambers they inhabit somewhat disjoint regions. For this reason chambers C1–C4 were filled with a "fast-gas" mixture of CF_4-isobutane to reduce their sensitivity to out-of-time hits. The downstream chambers C5–C8 were filled with an Argon-Ethane-isopropyl mixture, since less time resolution was needed. To accommodate the higher intensity planned for the 1999 run we intend to use the fast gas mixture in all chambers.

At the nominal intensity of $\sim$ 20 MHz the efficiencies across the chambers were high and relatively uniform, dipping only slightly in the beam region, as shown in Fig. 6.

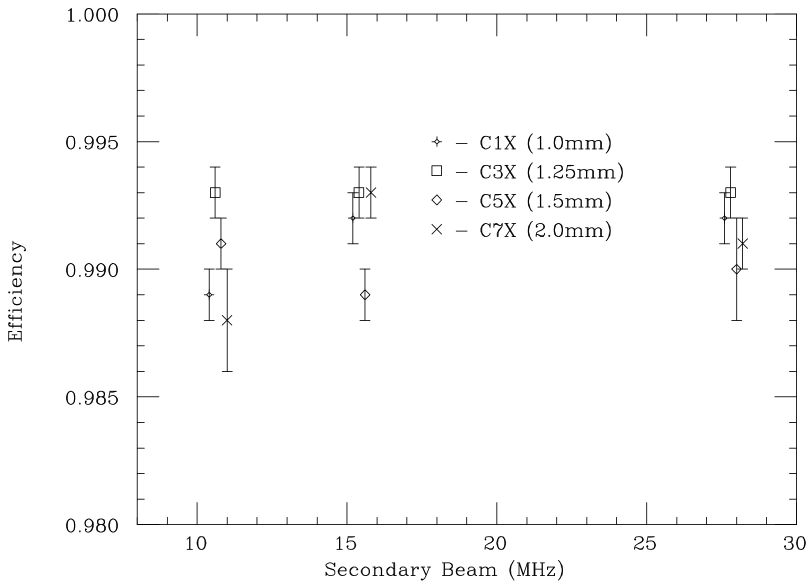

Figure 7: Chamber efficiency versus secondary beam intensities. Most of the running was at 20 MHz.

Furthermore, as seen in Fig. 7, the efficiencies were insensitive to intensity over the running range of the experiment.

In addition to its good timing properties, the CF_4-isobutane mixture is also known to mitigate the effects of aging. Over the course of the 1997 run a moderate amount of charge ($\sim$ 0.02C/cm) was accumulated along the wires in the beam region of the upstream chambers. Periodic monitoring of ^{55}Fe pulse amplitude in the beam region (see Fig. 8) has shown no indication of gain degradation of the anode wires due to aging. Another defense against aging is to operate the chambers at a low avalanche gain. Due to the low noise of the front-end system, the chambers achieve the efficiencies shown at an avalanche gain of only $\sim 4 \times 10^4$.

3.2 Trigger

A total of 24 triggers was used in the experiment, most for diagnostic and monitoring purposes. The triggers were fast, with single-bucket resolution (19 ns), simple, and provided high yields to tape. Only first-level triggers were employed. Common to all the physics triggers was a left-right coincidence of charged particles in the Same-Sign (as the channeled beam) and Opposite-Sign hodoscopes at the rear of the spectrometer. The addition of the hadronic calorimeter to the Cascade[3] and Kaon triggers reduced their rates by about a factor of six, with a very conservative minimum energy threshold. The typical Ξ-trigger rate was 30 kHz and the overall trigger rate including the Kaon,

[3]Calling it a Cascade trigger is a bit of a misnomer as it only requires two charged particles of opposite sign, and hence is really a Lambda trigger.

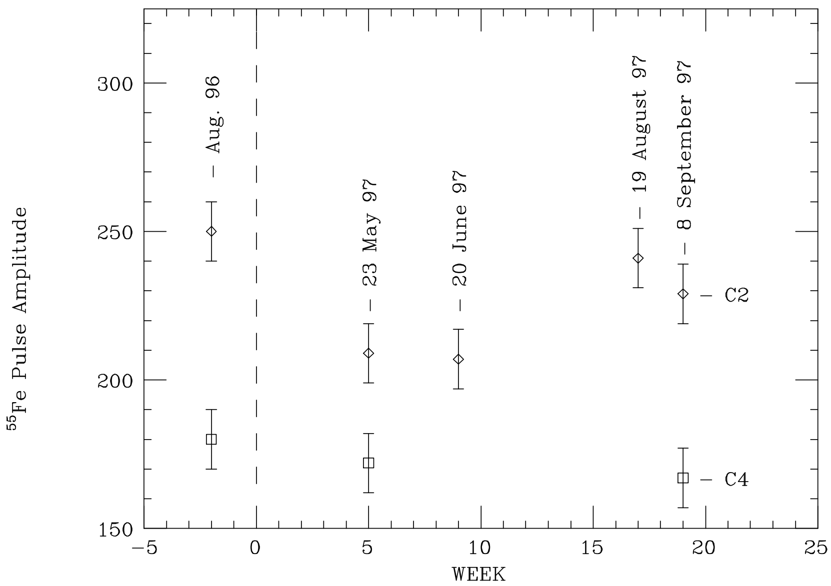

Figure 8: Gain vs time for chambers C2 and C4, measured with an ^{55}Fe source.

muon, and monitoring triggers was 75 kHz.

The trigger worked well and provided a high yield to tape. For example, typical Λ ($\overline{\Lambda}$) yields were 20% (5%) for the Cascade trigger. The trigger rate was about a factor of two higher than our Monte Carlo predictions, which is not surprising since the simulations did not include gamma conversions and particle production at the collimator exit. Every hodoscope element, sub-trigger, and trigger was scaled and written to disk by the slow DAQ, as well as being latched and written to tape by the fast DAQ.

3.3 Hadronic Calorimeter

The calorimeter is employed to provide a "muon blind" component to the standard left-right trigger and to reduce the trigger rate due to interactions in the spectrometer material. The calorimeter: 1) is fast, to avoid pile-up due to the high rate of interactions in the spectrometer, 2) has a sharp energy threshold, and 3) has the ability to detect muons. The calorimeter is $1\,\mathrm{m}^2$ in area and 9.6 interaction lengths long. All of the protons from Λ's decaying in the evacuated decay volume lie within a fiducial area of about half the calorimeter area.

The left hand plot in Fig. 9 shows the trigger efficiency as a function of energy of charged particles entering the calorimeter for a trigger threshold of about 50 GeV [4]. Note the sharp turn-on in acceptance. The right hand plot shows the total energy entering the calorimeter for charged particles of momentum between 100 and 120 GeV/c. Our preliminary (uncalibrated) estimate of the calorimeter resolution is: $\sigma/E = 80\%/\sqrt{E} + 2.5\%$.

[4] The minimum energy from a Λ decay proton is about 70 GeV.

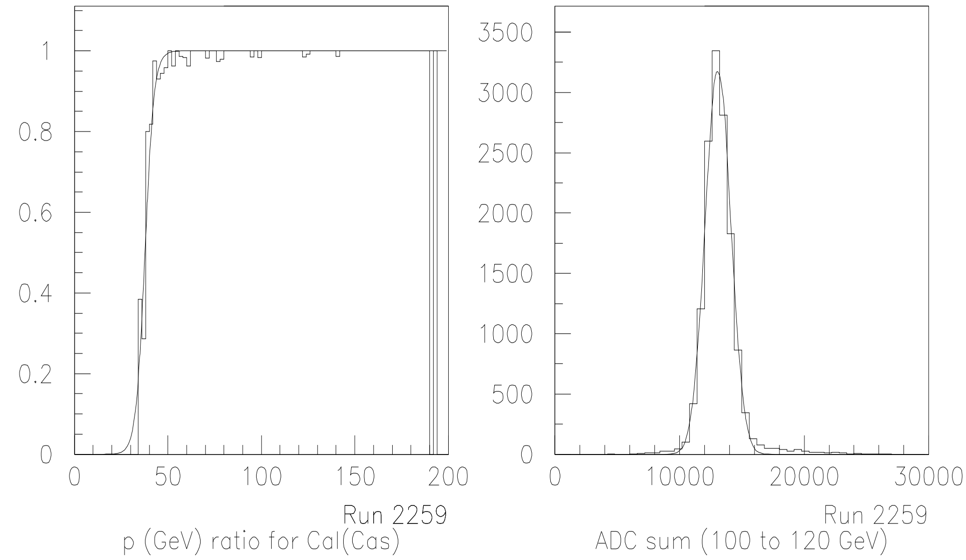

Figure 9: The left-hand plot shows the calorimeter trigger efficiency as a function of energy. The right hand plot shows the sum of the raw photomultiplier signals for all charged particles of momentum between 100 and 120 GeV/c.

3.4 Muon System

A muon station at the rear of the spectrometer was employed to allow rare and forbidden Hyperon decays to be accessed. (See Appendix A for more details on these physics topics.) The muon system is made up of two identical detectors, one on each side of the beam. Each consists of three stations (front, mid and rear) of proportional tubes separated by 0.81 m of steel. Each station contains an x and y readout plane. Two crossed scintillator hodoscopes following the rear proportional tube station provided triggering capability and helped to identify in-time proportional tube hits[5].

The proportional tubes use an Argon $-$ CO_2 (90/10) gas mixture. The efficiencies of the various muon detector elements, measured with beam, are shown in Fig. 10. Due to the wall thickness separating prop-tube cells, their efficiency is limited to $\sim 94\%$.

3.5 Data Acquisition System

The HyperCP data acquisition system is the fastest in the world, with a trigger rate of up to 80 kHz and a throughput to tape of 13 MB/s. Simplicity and parallelism are its hallmarks. The average dead time per event was 3 μs, and the average event size during standard running was 550 bytes. With the trigger rate listed above, HyperCP produced data at 44 MB/s during the spill for a continuous rate to tape of 13 MB/s. Tests with

[5]The proportional tube time resolution is limited to the total drift time since a simple latch read-out is used.

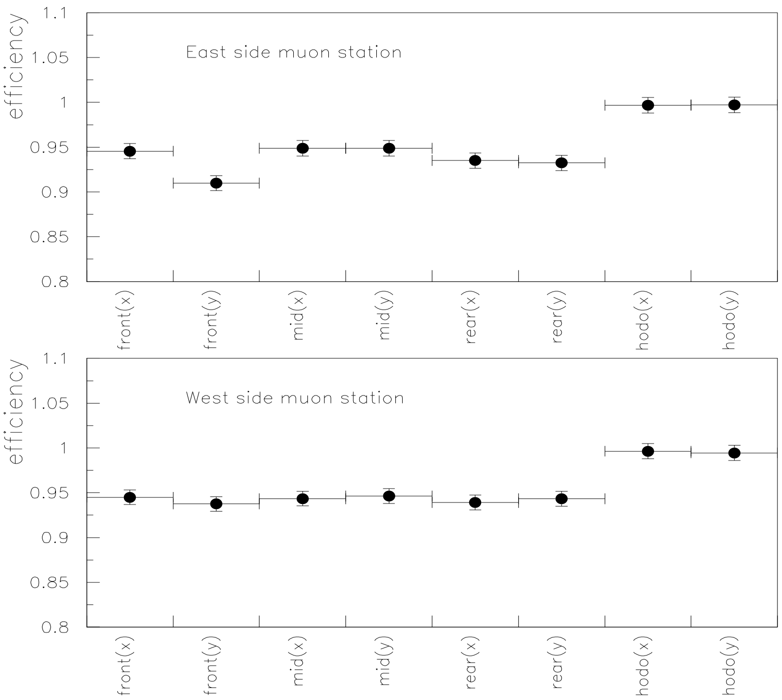

Figure 10: Average individual detector efficiencies of the muon system. The two rightmost points are the muon scintillator efficiencies whereas the other points are proportional tube efficiencies. Note that the maximum theoretical efficiency of the proportional tubes is 94% due to dead space between cells.

improved DAQ software made towards the end of the run gave a maximum sustainable data rate to tape of 17 MB/s.

Figure 11 shows the structure of the data-acquisition system. Information from the detectors was digitized and sparsified by two front-end systems: one based on the Nevis protocol and used to read out the wire chambers, latches and calorimeter ADC's, the other custom system designed by the Taiwan group and used to read out the muon chambers. The data were then transmitted via optical fibers to the VDAS (video data-acquisition system) spill buffers [19] in the control room. Five event-building systems operating in parallel accessed the VDAS to assemble events and record them on tape. Each event-building system was housed in a single VME crate and was composed of three MVME167 processors, five Event Buffer Interfaces (to provide access to the VDAS), and three Ciprico RF3573 SCSI host adapters [20] which each control three Exabyte 8505 tape drives [21]. Control of the system was provided via Ethernet links to each "Boss" MVME167 processor and to two booting and monitoring processors (not shown in the diagram) located in the Electronics Hall.

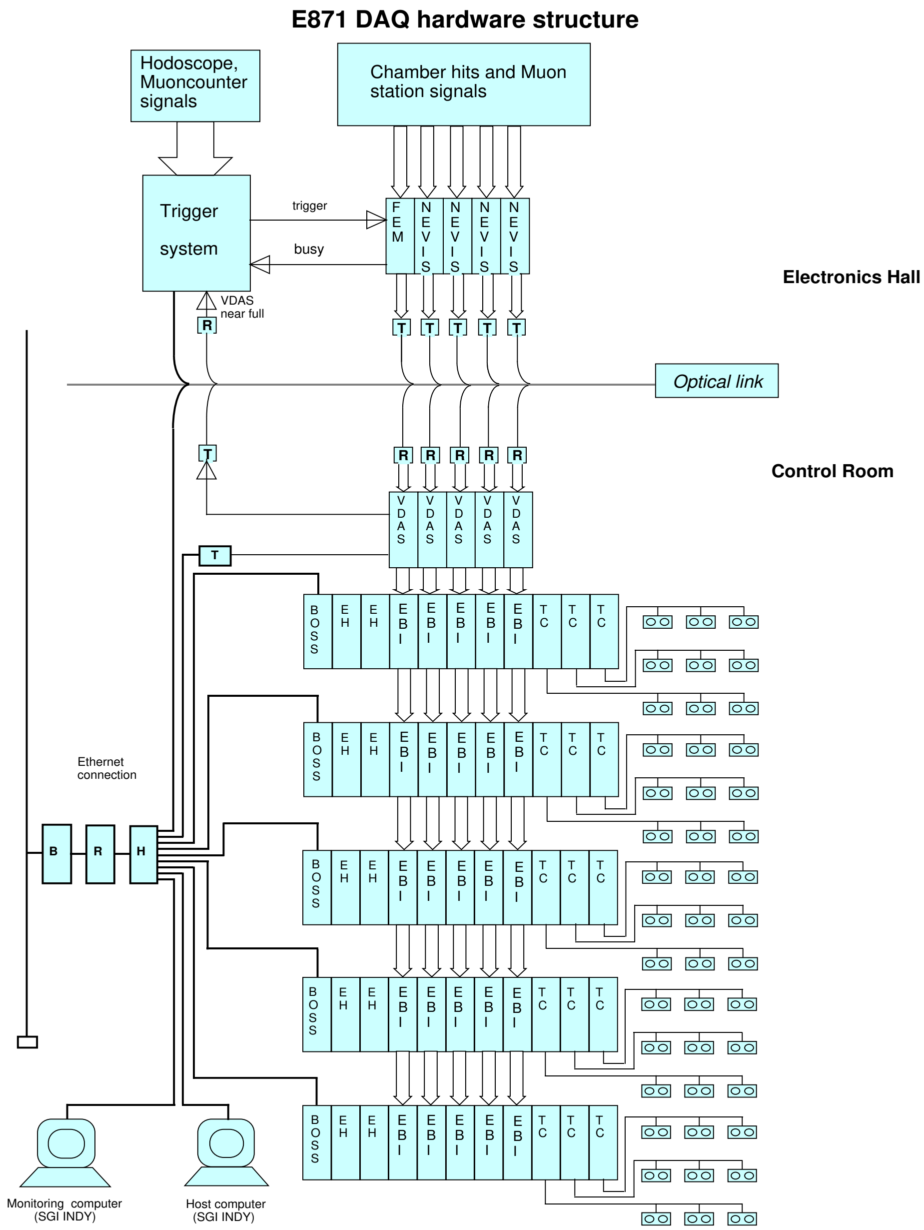

Figure 11: Block diagram of the HyperCP data acquisition system.

4 Synopsis of the 1997 Run

Although the fixed target run began in June 1996, because of our low priority, HyperCP did not receive beam until October 1996. After four months of beamline and spectrometer commissioning, the run officially began for HyperCP on April 4, 1997. Normal data-taking was completed after 16 weeks of running at the end of July[6] and was followed by systematic studies and special runs, which ended on September 5. The performance of the spectrometer improved continually throughout the run, and by the end of the run HyperCP was running at a high efficiency and consistently at our nominal beam intensity. The spectrometer worked as proposed. The only real surprise that we encountered is the fact that the $\overline{\Xi}^+$ production cross section is apparently about a factor of two lower than anticipated, which is part of the reason we did not accumulate as many $\overline{\Xi}^+$'s as expected.

A total of 75 billion events on 11,266 data tapes was accumulated during the run, with 63 billion events on 9,376 data tapes from the 16 weeks of normal data-taking. About twice as much time was spent running on positives than negatives because of the smaller $\overline{\Xi}^+$ yields.

The number of events written to tape and the yields are given in Table 3. We expect to reconstruct 1.6 billion $\Xi \to \Lambda\pi$ decays and 280 million $K^\pm \to 3\pi$ decays, as well as a large number of $\Omega \to \Lambda K$, and $K_s \to \pi^+\pi^-$ decays[7]. Since the statistical error in $A_{\Xi\Lambda}$ is given by:

$$\delta A_{\Xi\Lambda} = \frac{1}{2\alpha_\Xi\alpha_\Lambda}\sqrt{\frac{3}{N} + \frac{3}{\overline{N}}}, \qquad (12)$$

where N and $\overline{N}$ are the numbers of Ξ^- and $\overline{\Xi}^+$ events respectively, this sample of 2.84×10^8 $\overline{\Xi}^+$ and 1.31×10^9 Ξ^- events translates into an overall sensitivity of $\delta A_{\Xi\Lambda} \simeq 2 \times 10^{-4}$.

Further efforts at enhancing the Ξ yield by improving the reconstruction software and "rescuing" events in which one track has only its direction measured are underway.

5 Status of the Analysis of the 1997 Data

Since the end of the run we have concentrated our efforts on: 1) careful studies of the track reconstruction codes, 2) improving the event yield, 3) bringing up the farm code, and 4) making preliminary physics studies. Three different tracking codes using different algorithms were written and very carefully compared. Many other studies, such as measuring chamber efficiencies, magnetic field maps, alignment constants, etc., have been undertaken and are still in progress.

[6]However, three weeks were lost due to accelerator down time.

[7]The K_s's are produced by secondary beam interactions near the exit of the collimator.

Table 3: Total number of events written to tape and expected number of reconstructed events.

Events on tape			
	Channeled beam polarity		
Trigger	+	−	Total
Cascade	24.5×10^9	14.9×10^9	39.4×10^9
Kaon	40.8×10^9	21.3×10^9	62.1×10^9
All	48.8×10^9	25.6×10^9	74.4×10^9
Expected Number of Reconstructed Events			
	Channeled beam polarity		
	+	−	Total
$\Xi \rightarrow \Lambda\pi$	284×10^6	1310×10^6	1.59×10^9
$\mathrm{K} \rightarrow 3\pi$	204×10^6	75×10^6	279×10^6

5.1 Status of the Farm Data Processing

As Table 4 shows, the amount of computing power needed to reconstruct the events is quite large. Hence all of the primary data analysis will take place on the Fermilab farms. This analysis is underway and we expect that by the end of 1998, *and well before the beginning of the FY99 run*, all of the data will have been reconstructed.

The farm analysis began November 15 with one older, low-performance farm, `fnsfh` of two production systems utilizing 31 and 32 30-MIPS SGI Indy worker nodes. The efficiency for getting complete jobs through the original SGI systems has been very low due to a combination of hardware and software problems (not related to our code) which are not resolved as of this writing, despite the hard work of personnel in the Fermilab Computing Division.

On November 21 we were allocated two additional higher-performance farms: `fnsfo`, an SGI system with ten 114-MIPS workers, and `fnckm`, an IBM system with ten 115-MIPS workers. Our experience with these farms has been much better, and outside of a few startup problems we have run continuously on these systems.

With the current farm systems we have processed about 1% of the data. By February we hope to be ramped up to 10,000 MIPS. Our experience with the two higher-performance farms indicates that we can reconstruct about 45 million events per day on each farm. Hence with a 10,000 MIPS system we expect to be able to reconstruct about 375 million events per day, which corresponds to 200 days to reconstruct the entire 75 billion event data sample. Taking overhead into account, all the raw data should be processed in one calendar year.

We expect that the Monte Carlo analysis will take a further several months of time on the farms. Physics analysis will be conducted on machines at the home institutions,

Table 4: HyperCP 1997 run computing requirements.

Process	Events	Analysis time (MIPS-sec) Per event	Total
Raw data processing	75×10^9	2.0	150×10^9
Physics analysis	5×10^9	0.2	1×10^9
Monte Carlo studies	5×10^9	4.0	20×10^9
Total:			170×10^9

where there are about 4,000 MIPS of computing power available.

5.2 Preliminary Results

In what follows we show some plots that give an indication of the quality of the data. All of these results are preliminary, as we continue to work on the code and constants, and come from a tiny fraction of the data.

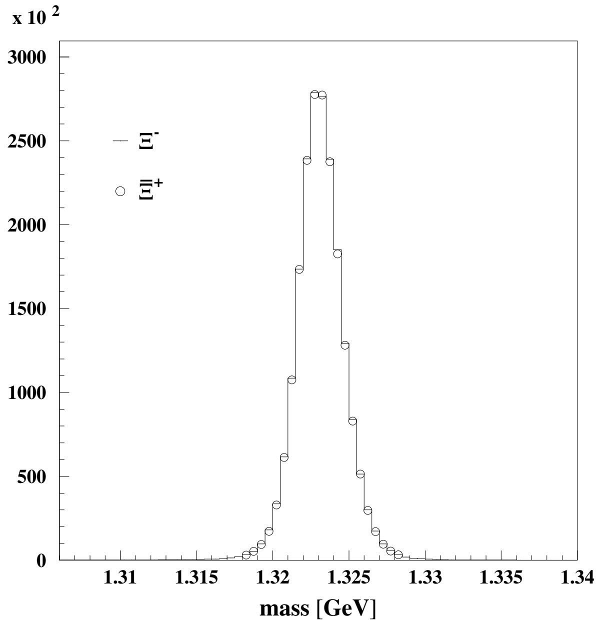

Figure 12: $\Lambda\pi$ invariant mass for negative and positive Ξ-trigger events. The mass resolution is 1.5 MeV/c^2.

A normalized comparison of the $\Lambda\pi^-$ and $\overline{\Lambda}\pi^+$ masses, based on some 2 million reconstructed Ξ^- and 0.5 million $\overline{\Xi}^+$ events, processed by the farms, is shown in Fig. 12.

The excellent mass resolution of $\sigma = 1.5\,\mathrm{MeV/c^2}$ is already at the level expected from the Monte Carlo. The level of the background is considerably less than 10^{-3}. As the background is thought to be mainly poorly measured Ξ's, improvements in the magnetic field parametrization and alignment constants will reduce it further.

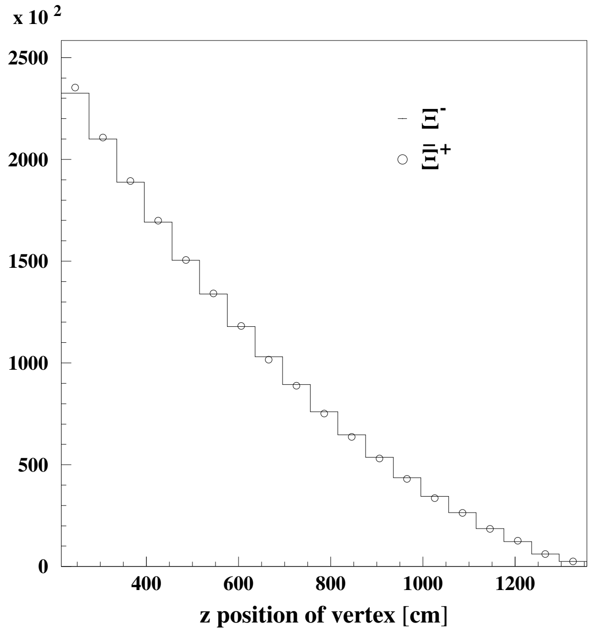

Figure 13: Decay vertex distribution for Ξ^- and $\overline{\Xi}^+$ events.

Figure 13 shows the distributions of the Ξ^- and $\overline{\Xi}^+$ decay vertices. The agreement is excellent. No acceptance corrections have been made in this or any other plot. Figure 14 shows the $\pi^\pm\pi^\pm\pi^\mp$ invariant mass in the region of the $\mathrm{K}^\pm$ mass. The mass resolution of 2.7 $\mathrm{MeV/c^2}$ is again consistent with Monte Carlo estimates. Figure 15 shows a comparison of Ω^- and $\overline{\Omega}^+$ masses as measured through their $\Lambda\mathrm{K}$ decay products. The agreement in mass *and background level* is again striking. Finally, we note that approximately 1% of our triggers is from the $\pi^+\pi^-$ decays of K_s's produced near the exit of the collimator, which provides us with a running calibration of the spectrometer magnetic field. The resultant $\pi^+\pi^-$ invariant mass distribution is shown in Fig. 16.

In Fig. 17 we show the preliminary *uncorrected* distributions of the cosine of the polar angle that the proton (anti-proton) makes with respect to the Λ ($\overline{\Lambda}$) polarization in the Λ ($\overline{\Lambda}$) helicity frame — the key comparison in finding a CP-violating effect in our experiment. The errors are negligible compared to the size of the symbols used. *Again, we emphasize that no acceptance corrections have been made.* The approximate linearity shows illustrates the excellent acceptance over the full polar angle range. The two distributions are clearly comparable. A detailed analysis of these events, which represents less than one day of running, would already establish CP invariance at a statistical level about an order of magnitude better than the best published result.

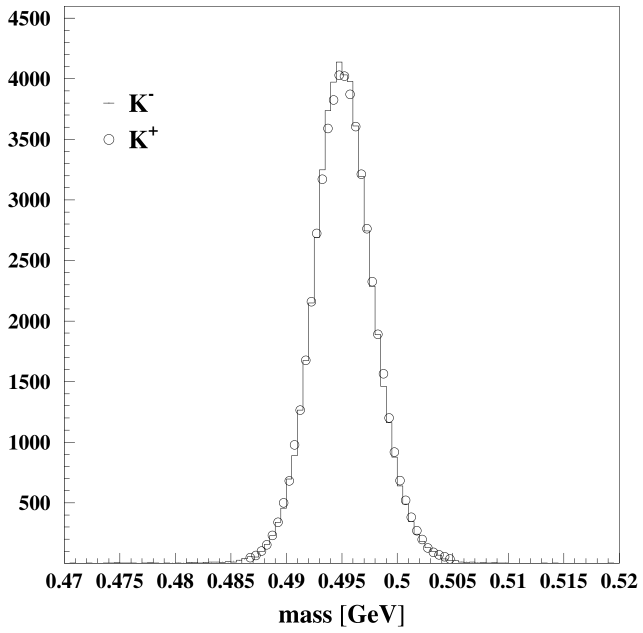

Figure 14: The $\pi^{\pm}\pi^{\pm}\pi^{\mp}$ invariant mass for positive and negative K-trigger events. The mass resolution is 2.7 MeV/c^2.

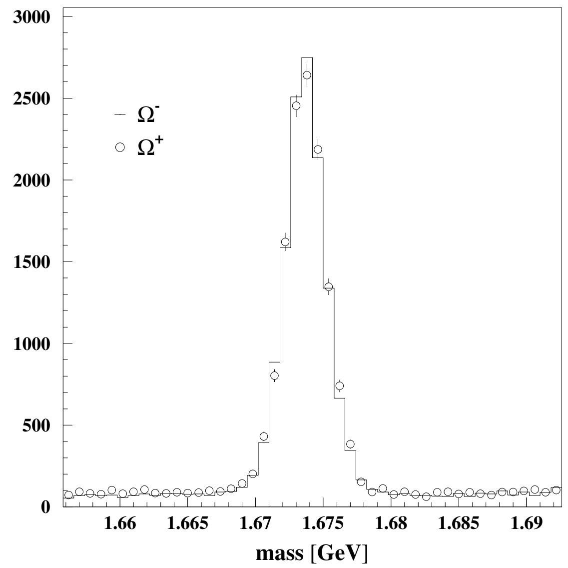

Figure 15: ΛK mass distributions for events after kinematic and geometric fit. The mass resolution is 1.5 MeV/c^2.

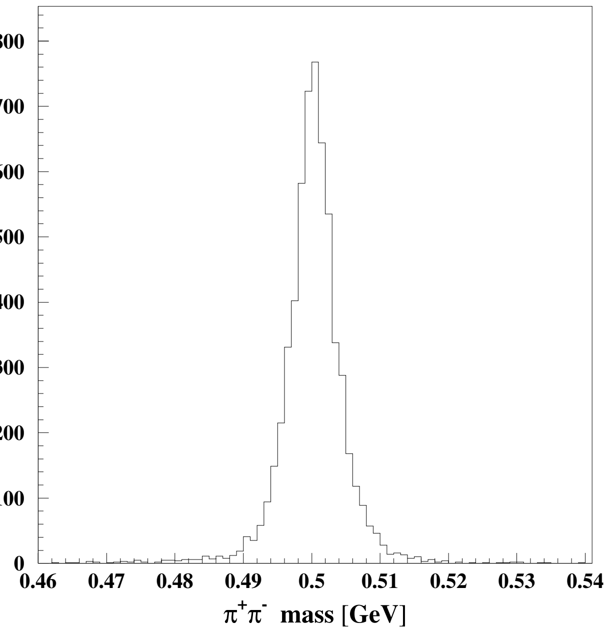

Figure 16: Distribution of $\pi^+\pi^-$ mass. The mass resolution is 4.6 MeV/c^2.

We have started studying the systematic effects that were addressed in the original proposal, and which are summarized in Appendix B. Although the previous results are quite promising, and show no indication of biaes, these studies are still quite immature.

In addition to searching for CP violation in Ξ and Λ decay, there are several analysis efforts going in parallel that address other physics topics. These are briefly discussed in Appendix A.

6 FY99 Run

The Fermilab draft long-range schedule of November 1997 has the Tevatron fixed-target run beginning April 1, 1999, with 8 weeks of startup and 20 weeks of fixed-target beam. In what follows, we assume a 16 week run with normal data-taking followed by a 4 week series of systematic studies.

6.1 Sensitivity in CP violation for the FY99 Run

With the commissioning of the Main Injector, the upcoming 800 GeV fixed target program in FY99 will allow us to meet and exceed the original goals of HyperCP. Most of the improvement will come from accruing more data by running more efficiently and at a higher intensity. In the 1997 run we started with a rather low intensity and efficiency. Merely running at the intensity and efficiencies that we routinely achieved during the last month of the run will increase our yield by about a factor of three. A better duty

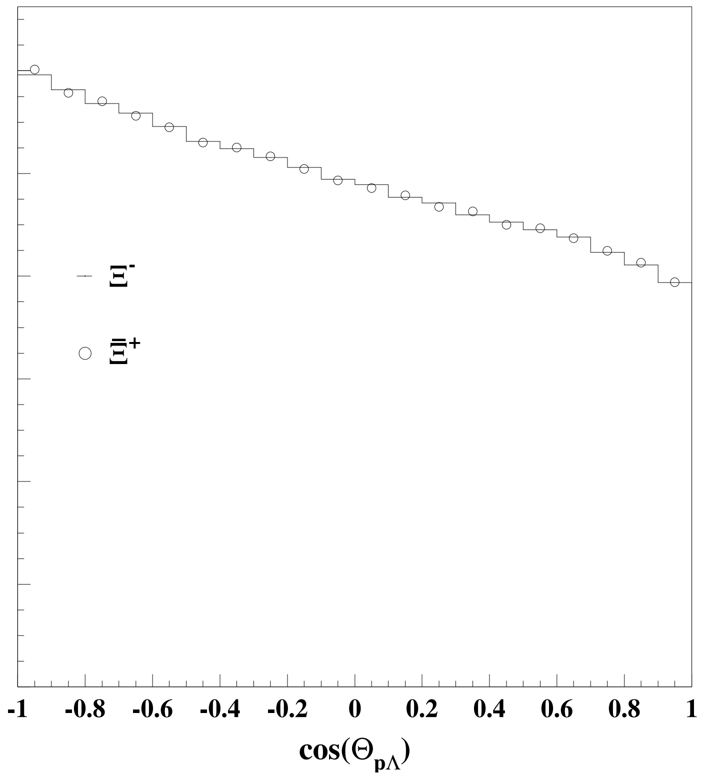

Figure 17: Distribution of cosine of the angle $\theta_{p\Lambda}$ between the momentum of p($\overline{\mathrm{p}}$) and the $\Lambda(\overline{\Lambda})$ polarization in the $\Lambda(\overline{\Lambda})$ rest frame.

factor and a slight increase in intensity will increase that to at least a factor of four. If offline studies show no degradation in the quality of the special high-intensity data we took in 1997, then we could increase that factor to about six before DAQ bandwidth and radiation safety become limiting factors. Note that the length of the FY99 run should be almost the same as our official 1997 run, which lasted from the beginning of April until the end of July, but which had three weeks of accelerator down time. However, it is imperative that we hit the ground running, which given the modest changes we will make to the apparatus, should be feasible.

Combining the samples of 1997 and FY99 runs, the projected statistical uncertainty in $A_{\Xi\Lambda}$ is 9×10^{-5} or better. In addition to increasing the data volume, the data quality will be improved with minor, but significant, improvements in the apparatus, monitoring software, and better understanding of our spectrometer.

Table 5 is a comparison of the running conditions between the 1997 run and the FY99 run. We intend to increase the nominal proton intensity by a factor of 1.33 from what it was at the end of the 1997 run, corresponding to a secondary beam rate of 25 MHz for the upcoming run. As shown in Fig. 7, this conservative increase in intensity will have very little effect in the performance of the spectrometer. Indeed, we have run at

	1997 run	FY99 run
Nominal intensity (protons/s)	7.5×10^9	1.0×10^{10}
Channeled beam rate (MHz)	20	25
Spill duty factor	18s/60s	40s/80s
Calendar time (Weeks)	16	16
Mean 'efficiency' (%)	28	50
Effective total number of spills	44,440	60,480
Total number of protons	6×10^{15}	2.4×10^{16}

Table 5: Comparison of protons on target for the 1997 and FY99 runs, excluding special data-taking runs.

even higher intensities. Increased backgrounds are holding us back from running at even higher intensities.

It is proposed that the Tevatron will have a 40 second spill followed by a 40 second interspill period in the FY99 run, for a 50% duty factor. The duty factor in the 1997 run was 30%, which means that, for a given intensity, a gain of 1.66 in yield is achieved.

The 'efficiency' given in Table 5 is the product of two factors: 1) the fraction of total spills that we wrote good data to tape, and 2) the fraction of the nominal beam intensity at which we ran. For the 1997 run it is calculated by dividing the total amount of protons incident on target during normal data-taking by the number of protons we would have taken had we run at the nominal beam intensity 24 hours a day for the entire period. Hence the 'efficiency' includes accelerator down-time, which was about three weeks in the 1997 run, our own inefficiencies, and the less than nominal intensities at which we ran at the beginning of the official run. We expect to have an overall 'efficiency' in FY99 of 50% — what we routinely achieved at the end of the 1997 run — for a gain of 1.78 in yield.

With these gains we will accumulate a factor of four more data in FY99 than in our first run. And as we continue to explore the intensity-and-yield limit of our experiment based on data on tape, it is quite feasible that we can do better than a factor of four.

6.2 Improvements for the FY99 Run

Although the apparatus worked remarkably well, particularly given the tight fabrication schedule and minimum commissioning time, a number of areas of improvement has been identified. The major area of improvement is an increase in the speed of the fast data acquisition system, where our intention is to double the throughput to tape.

The modifications are itemized below. Not listed is a host of minor, but significant improvements that require a minimum of funding and effort. Nevertheless, these improvements taken in aggregate, will substantially improve the quality of the data.

- **Data acquisition modifications.**

  Some of the improvements to the data acquisition system have already been designed and tested. These include reducing the event size, tape-writing via the SCSI bus on the single-board computers, and switching to the new Exabyte 8705 tape drives.

  The maximum rate we could write to tape in the 1997 run, 13 MB/s, was limited by software inefficiencies. Improved software was tested towards the end of the run which will allow a rate of 17 MB/s, close to the theoretical maximum throughput of the tape drives. The effective rate can also be improved by a data compression scheme for the wire chamber data. Such a scheme exists in software and reduces the event size by about 30%. Implementation of this scheme in the hardware (before the VDAS buffers) is straightforward.

  With data compression in place, the average event size for the FY99 run will be 385 Bytes, as shown in Table 6. Since the trigger rate will be about 100,000 Hz, we will acquire 1.54 GB of data in every 80-s spill. This translates to a minimum DAQ throughput of 19 MB/s for writing all events to tape in 80 s. This requirement is beyond the capability of the 45 Exabyte 8505 tape drives in the 1997 DAQ system. This, coupled with the fact that the Exabyte 8505 tape drives we used in the 1997 run have been heavily used and are worn out, dictates replacing them with the new Exabyte 8705 drives that use the same tape medium but have a throughput of 1 MB/s.

  By upgrading the real-time operating system to VxWorks 5.3, the tape drives can be connected directly to the SCSI bus on the MVME167 single-board computers, reducing the traffic congestion on the VME back plane. This is an option not available with VxWorks 5.1. Figure 18 shows the results of a test driving three Exabyte-8705 tape drives from one SCSI port of a MVME167. It is clear that we can achieve a throughput of about 40 MB/s with three Exabyte 8705 drives on each of the fifteen MVME167 computers that we have in our existing DAQ.

  We also intend to reduce the dead-time of the front-end readout electronics. This will be done by increasing the speed of the readout clock, reducing the event size by limiting the maximum number of latched words per crate, and re-routing the gating system.

  The upgraded DAQ system for the FY99 run should have enough headroom to allow for beam intensities beyond what we stated in Sec. 6.1.

- **Collimator modifications.**

  There are indications that the collimator was misaligned resulting in the loss of some fraction of the secondary beam. We are currently using data to understand the misalignment and to correct the problem for the 1999 run. We will also take the opportunity to modify parts of the collimator to eliminate a hot spot producing

	1997 run	FY99 run
Trigger rate (Hz)	75,000	100,000
Event size (Bytes)	550	385
Data volume per spill (MB)	825	1540
DAQ throughput (MB/s)	13	19
Total number of spills	44,440	60,480
Total number of events (billion)	63	242
Total data volume (TB)	33	93
Number of 5-GB tapes	9,376	20,000

Table 6: Specifications of the DAQ for the 1997 and FY99 runs, excluding special data-taking runs.

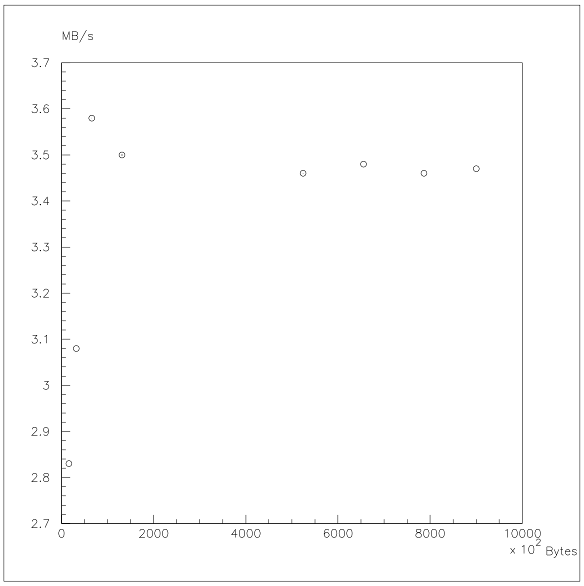

Figure 18: Throughput of Exabyte 8705 tape drive as a function of the data-block size. Three Exabyte 8705 drives in compressed mode were used with one MVME 167 single-board computer.

tertiary particles and to minimize the thermal stress in the two high-precision Hall probes located near the exit of the channel (which knocked out their temperature sensors).

- **Preamplifier modifications.**

  The preamps on one of the large chambers downstream of the analysis magnet would occasionally break into oscillation during bursts of high instantaneous beam intensity. A simple retrofit by back-terminating the preamplifier outputs will alleviate this problem.

- **Minimum bias trigger modifications.**

  Our minimum bias events were collected with a simple secondary beam counter that could only handle low intensity. We plan to replace it with a coarsely segmented scintillating fiber hodoscope.

- **Target SWIC modifications.**

  During the run, the two 0.5 mm-pitch target SWICs developed a few dead or inefficient channels in the critical region for monitoring the incident angle of the proton beam. They should be replaced for the 1999 run.

- **Air conditioning modifications.**

  There are two air conditioning units in MC7 for cooling the preamplifiers and discriminators of the wire chambers. These units did not have enough capacity. With improved air conditioning in this area the rate of electronic failure will drop significantly. This, in turn, will increase our run time efficiency by reducing the number of accesses to MC7 for replacing bad cards.

6.3 Analysis of the FY99 Data

The amount of data we will need to analyze is estimated in Table 7. We expect to take 240 billion events of normal data and about 35 billion events for special studies. Because of improved data compaction and more efficient utilization of tape, we expect to write about 20,000 tapes, or only about a factor of two more than we wrote in the 1997 run. The total number of events will be increased by a factor of four, *if we keep the trigger fractions the same*. The Cascade trigger faction, which was about 50% in the 1997 run, could be increased to about 75% by prescaling some of the other triggers (and sacrificing some of the other physics). This would reduce the number of events written to tape by 25%. However, we assume throughout this proposal that the trigger fractions remain the same as in the 1997 run.

To analyze this data we request 20,000 MIPS of Fermilab farm nodes beginning in January, 2000. Assuming that our reconstruction program runs at its current speed, it should take 400 days to reconstruct all of the data.

6.4 Cost Estimate and Schedule

Institutional responsibilities will be the same as in the 1997 run. The responsibilities for the apparatus modifications and cost estimates are given in Table 8. Most of the funding for the upgrades will come through the DOE via the collaborating institutions. Fermilab will be responsible for the modifications to the collimator, and associated rigging.

Table 7: HyperCP FY99 run computing requirements.

Process	Events	Analysis time (MIPS-sec) Per event	Total
Raw data processing	275×10^9	2.0	550×10^9
Physics analysis	20×10^9	0.2	4×10^9
Monte Carlo studies	20×10^9	4.0	80×10^9
Total:			634×10^9

Table 8: HyperCP FY99 cost estimate.

Cost Estimate for the FY99 Run				
Project	Institution	Number	Cost	Total
Preamp retrofit	UVa	500	$20	$10,000
Replacement:MQS104 preamp chips	UVa	60	$50	$3,000
Replacement:MVL107 disc. chips	LBNL	100	$20	$2,000
Replacement:ADC chips	UVa	2	$500	$1,000
Calorimeter trigger module	UVa	1	$2,000	$2,000
Secondary beam counter	USA	1	$8,000	$8,000
DAQ upgrade (including tape drives)	IIT, LBNL, Taiwan	1	$100,000	$100,000
Collimator modifications	FNAL, LBNL	1	$10,000	$10,000
Hall probe replacement	FNAL	2	$3,000	$ 6,000
Subtotal:				$132,000

APPENDIX

A Other Physics

We have built a world-class charged hyperon beam and spectrometer which allows other physics topics to be addressed besides the CP violation in hyperon decays. Most of these will be studied with unprecedented sensitivity. These are briefly described below.

- **CP violation in $K^{\pm} \to 3\pi$ decays.**
We have accumulated 280 million $K^{\pm} \to \pi^{\pm}\pi^{\pm}\pi^{\mp}$ decays which will allow CP to be tested through the asymmetry in the slope parameter of the Dalitz plot. We expect a statistical precision of about 6×10^{-4}, an order of magnitude better than the current limit [22]. Theoretical predictions range from 1.4×10^{-3} to about 10^{-6} [23, 24, 25, 26].

- **Flavor changing neutral currents in hyperon decays.**
No experiment has ever observed strangeness-changing neutral currents in hyperon decays such as $\Sigma^+ \to p\mu^+\mu^-$. Our single event sensitivity will be about 10^{-9}.

- **Flavor changing neutral currents in charged kaon decays.**
The decay $K^+ \to \pi^+\mu^+\mu^-$ has recently been observed by E787 at BNL at a branching ratio of about 5×10^{-8}. HyperCP should see a few tens of these decays and confirm their result.

- **Lepton number nonconservation in kaon and hyperon decays.**
Why total lepton number seems conserved is not understood and remains a question of fundamental importance. HyperCP addresses this problem through the $|\Delta L| = 2$ decays: $\Sigma^- \to p\mu^-\mu^-$ and $\Xi^- \to p\mu^-\mu^-$, as well as through the associated kaon decay: $K^+ \to \pi^-\mu^+\mu^+$. We will improve the current limits by four orders of magnitude to about 10^{-8}.

- **Measurement of the β parameter in Ξ decays.**
The experiment accumulated a large amount of polarized Ξ^- and $\overline{\Xi}^+$'s by running at non-zero production angles. Measurement of the β term in equation (5) allows a determination of the strong phase shifts in Ξ decay through the relationship:

$$\frac{\beta}{\alpha} = -\tan(\delta_3^S - \delta_3^P),$$

where δ_3^S and δ_3^P are respectively the S- and P-wave strong phase shifts. This will allow the recent theoretical predictions of the phase shift, which differ significantly from earlier calculations, to be tested. Note that a small value for the phase shifts would imply that the asymmetry $A_{\Xi\Lambda}$ is dominated by CP violation in Λ decays.

- **Measurement of the polarizations of the Ξ^-, $\overline{\Xi}^+$, Ω^-, and $\overline{\Omega}^+$, and magnetic moments of Ξ^- and $\overline{\Xi}^+$hyperons.**
  Why hyperons are produced polarized in high energy interactions remains a mystery. HyperCP will study Ξ^- and $\overline{\Xi}^+$polarization at low x_F and p_T where there are little data, as well as the Ω^- and $\overline{\Omega}^+$ polarizations. Previous experiments concluded that if Ω^- is polarized, its magnitude must be small, and no experiment has measured the $\overline{\Omega}^+$ polarization. A byproduct of this will be precision measurements of the Ξ^- and $\overline{\Xi}^+$magnetic moments.

- **Production cross sections for π^-, K^-, Ξ^-, and Ω^- and antiparticles.**
  It is important that HyperCP address this topic. It is already apparent that the $\overline{\Xi}^+$cross section is significantly smaller than anticipated. We have data with different targets and production angles which will allow cross sections at low x_F and p_T to be measured.

- **Tests of CPT.**
  The excellent mass resolution and large data sample will allow precise tests of CPT through comparison of the masses and lifetimes of the Ω^-, Ξ^-, Λ^0, K^+, and their associated antiparticles.

B Systematic Errors

A precision measurement can only be successful if systematic effects can be controlled and understood. In general, we have identified four categories of potential sources of bias: (1) acceptance differences between Ξ^- and $\overline{\Xi}^+$ decays, (2) non-zero polarization of the parent Ξ, (3) differences in the particle anti-particle interaction rate within the spectrometer (*i.e.*, p versus $\overline{p}$, and π^- versus π^+ interaction cross sections), and (4) different backgrounds under the Λ and $\overline{\Lambda}$ and the Ξ^- and $\overline{\Xi}^+$ mass peaks.

Because the α parameters for the Ξ and Λ both change sign under CP, the proton decay distribution in the Λ rest frame should be identical to the anti-proton decay distribution in the $\overline{\Lambda}$ rest frame (assuming the parent Ξ's are unpolarized and CP is conserved). In principle, since both magnet polarities are flipped, no acceptance corrections are required! Implicit is that the magnetic fields, detector components, and reconstruction efficiencies remain stable between positive and negative running. To facilitate this stability, the magnetic polarity is changed frequently (about every four hours at full beam intensity), the magnetic fields are monitored with high-precision Hall probes, and an approximately uniform secondary beam flux is maintained by using different length targets. Given that real experiments are never ideal, acceptance variations will be tracked and corrected.

It should be emphasized that absolute normalizations are not important: for example, a *uniform* difference in chamber efficiency from Ξ^- to $\overline{\Xi}^+$ running would produce no bias. Crucial to the elimination of biases is the analysis method. Because the Λ direction in the Ξ rest frame changes from event to event, so too does the direction of the Λ polarization and hence the analysis frame in which the proton polar angle is measured (see Fig. 19).

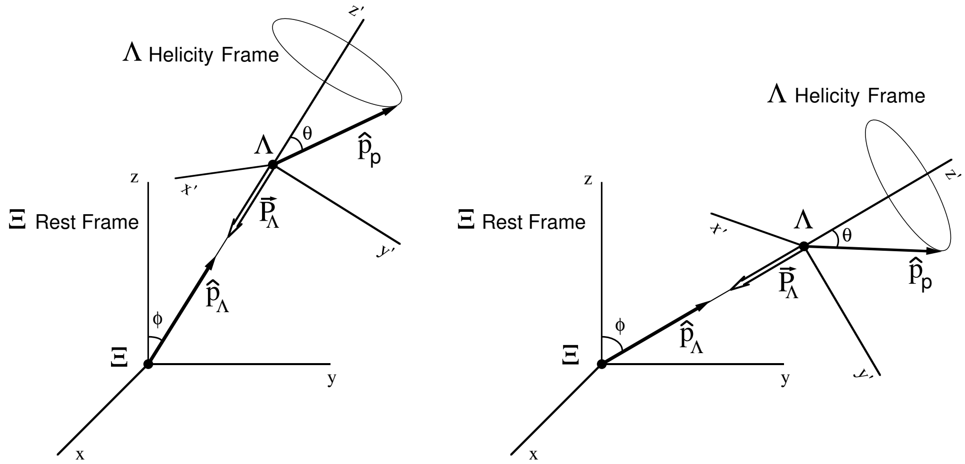

Figure 19: Two Ξ decays with identical proton polar angles θ in the Λ helicity frame, but different directions in the laboratory.

As a consequence, acceptance differences localized to a particular part of the apparatus only weakly map to a particular part of the proton or antiproton angular distribution, from which $\alpha_\Lambda \alpha_\Xi$ is extracted. Indeed, in the limit of uniform Λ acceptance, any correlation at all would vanish.

Because of mistargeting and the finite size of the hyperon channel, some parent Ξ's may be produced with non-zero polarization. The magnitude of this polarization, although expected to be quite small, if not zero, will be measured and any bias can, in principle, be removed (if required). For these events, the parent Ξ will have a small, fixed polarization in the lab frame; however, in the Λ helicity frame, the effects of this polarization will be diluted as discussed above. Special runs with measurable Ξ polarizations were taken to calibrate this effect.

Finally, differences in particle and anti-particle interaction cross sections are currently being studied. Small corrections may be required but we expect to understand this bias to better than $\sim 1 \times 10^{-4}$.

C MicroMegas Chambers

We are investigating the possibility of replacing the upstream wire chambers with a new system with better rate capability and resolution. Charpak, Giomataris, *et al.,* [27] are developing a new kind of high-rate asymmetric wire chamber, dubbed "MicroMegas" due to its use of a nickel micromesh as one electrode in a parallel-plate gas-amplification structure. The asymmetric structure provides sufficient gas thickness (3 mm) for efficient detection of minimum-ionizing tracks while keeping the amplification gap small (100 μm) to allow fast ($\approx$100 ns) clearing of the positive ions. Rate capability in excess of 10^5 particles/mm^2/s has been demonstrated with no evident aging effects. MicroMegas chambers can be constructed out of very little material: there are no wires, the $\approx$50%-transparent micromesh is only 3 μm thick, and the remaining elements are kapton foils and a sparse array of small plastic spacers.

MicroMegas chambers of $25\times25\,\mathrm{cm}^2$ active area are now available from the Eurisys company, and one will soon be delivered to Berkeley for testing and evaluation. Eurisys has also quoted on production of $40\times40\,\mathrm{cm}^2$ detectors, which would be suitable for replacing some of the MWPCs upstream of the analyzing magnets. Such replacement would both lessen the confusion due to track overlap and improve rate capability in that critical region of the spectrometer where hyperon-decay tracks can overlap with each other and with secondary-beam tracks. If after evaluation these chambers are found to be a workable solution, we will consider whether such an apparatus upgrade is appropriate given the time available for shakedown prior to the beginning of the 1999 run.

References

[1] T.D. Lee and C.N. Yang, Phys. Rev. **108** (1957) 1645.

[2] G. Valencia, private communication.

[3] J.F. Donoghue, X.-G. He and S. Pakvasa, Phys. Rev. D**34** (1986) 833.

[4] L.D. Roper, R.M. Wright, and B.T. Feld, Phys. Rev. **138** (1965) 190.

[5] M. Lu, M.B. Wise, and M.J. Savage, Phys. Lett. **B337** (1994) 133.

[6] A. Datta and S. Pakvasa, Phys. Lett. **B344** (1995) 430.

[7] D. Chang, X.-G. He, and S. Pakvasa, Phys. Rev. Lett. **20** (1995) 3927.

[8] M. Shifman, A. Vainshtein, and V. Zakharov, Nucl. Phys. **B120** (1977) 316.
F. Gilman and M. Wise, Phys. Lett. **B93** (1980) 129.

[9] X.-G. He and S. Pakvasa, in Proceedings of the 8the Meeting Division of Particles and Fields of the American Physical Society, edited by S. Seidel (World Scientific, Singapore, 1995), pp. 984–990.

[10] N.G. Deshpande, X.-G. He, and S. Pakvasa, Phys. Lett. **B326** (1994) 307.

[11] X.-G. He and G. Valencia, *CP Violation in* $\Lambda \to p\pi^-$ *Beyond the Standard Model*, Phys. Rev. D**52** (1995) 5257.

[12] H. Albrecht, *et al.*, "The Interest in Studying Beauty Baryon in pN Interactions at HERA", DESY 93–156.

[13] X.-G. He, H. Steger and G. Valencia. Phys. Lett. **B272** (1991) 411.

[14] J.M. Flynn and L. Randall, Phys. Lett. **B224** (1989) 221.

[15] E.A. Paschos and Y.L. Wu, Mod. Phys. Lett. **A6** (1991) 93.

[16] P. Chauvat et al., Phys. Lett. **163B** (1985) 273.

[17] M.H. Tixier et al., Phys. Lett. **B212** (1988) 523.

[18] P.D. Barnes et al., Phys. Rev. C**54** (1996) 1877.

[19] A. E. Baumbaugh *et al.*, IEEE Trans. Nucl. Sci. **NS-33**, 903 (1985); K. L. Knickerbocker *et al.*, IEEE Trans. Nucl. Sci. **NS-34**, 245 (1986).

[20] Ciprico, 1161 Homestead Ln., Chanhassen, MN 55317.

[21] Exabyte Corp., 1685 38th Street, Boulder CO 80301.

[22] W.T. Ford et al., Phys. Rev. Lett. **25** (1970) 1370.

[23] B. Grinstein, S.J. Reg, and M.B. Wise, Phys. Rev. D**33** (1986) 1495.

[24] A.A. Bel'kov et al., Phys. Lett. **B300** (1993) 283.

[25] G. D'Ambrosio, G. Isidori, and N. Puver, Phys. Lett. **B273** (1991) 497.

[26] H.-Y. Cheng Phys. Rev. D**44** (1991) 919.

[27] Y. Giomataris et al., NIM A 376,29 (1996).